Spatial and Temporal Structure of Edge-Localized Modes

A. Kirk,[1] H. R. Wilson,[1] G. F. Counsell,[1] R. Akers,[1] E. Arends,[1,2] S. C. Cowley,[1,3] J. Dowling,[1] B. Lloyd,[1] M. Price,[1] M. Walsh,[1,4] and MAST Team[1]

[1]*EURATOM/UKAEA Fusion Association, Culham Science Centre, Abingdon, Oxon OX14 3DB, United Kingdom*
[2]*FOM-Institute for Plasma Physics "Rijnhuizen", Edisonbaan 14, NL-3439 MN Nieuwegein, The Netherlands*
[3]*Imperial College of Science and Technology, University of London, London SW7 2BZ, United Kingdom, and Department of Physics and Astronomy, UCLA, Los Angeles, California 90095, USA*
[4]*Walsh Scientific Ltd., Culham Science Centre, Abingdon, Oxon OX14 3EB, United Kingdom*

(Received 21 January 2004; published 16 June 2004)

This Letter provides information on the spatial and temporal structure of periodic eruptions observed in magnetically confined laboratory fusion plasmas, called edge-localized modes (ELMs), and highlights similarities with solar eruptions. Taken together, the observations presented in this Letter provide strong evidence for ELMs being associated with a filamentlike structure. These filaments are extended along a field line, are generated on a 100 μs time scale, erupt from the outboard side, and connect back into the plasma. Such structures are predicted by a theoretical model based on the "ballooning" instability, developed for both solar and tokamak applications.

DOI: 10.1103/PhysRevLett.92.245002 PACS numbers: 52.35.Py, 52.55.Fa, 52.55.Rk

The edge-localized mode (or ELM) is a repetitive instability associated with a steep pressure gradient, which can form at the edge of a tokamak plasma in high confinement regimes [1,2]. Similar to solar eruptions, ELMs are explosive events, which eject large amounts of energy and particles from the confined region [2]. Understanding the poloidal and toroidal localization and the outward radial extent of ELMs is crucial in order to calculate their effect on power loading both on the first wall and the divertor target plates in future devices. Theoretical models based on the so-called ballooning mode [3] have been proposed independently for both ELMs [4] and solar flares [5]. The mode is destabilized when the plasma pressure gradient exceeds a critical value. This value is close to that measured in the tokamak plasma edge [6], providing an indication that the ballooning mode plays a role in ELMs. In this Letter, detailed measurements of the spatial and temporal structure of ELMs observed in the MAST [7] tokamak (at Culham Science Centre, UK) will be presented, which confirm a number of predictions of the nonlinear ballooning mode theory [8,9]. In particular, this theory predicts that a ballooning mode will evolve into a filamentary structure, which is highly elongated along the magnetic field lines. Even close to the linear marginal stability boundary, the instability is predicted to grow explosively. Each filament narrows and twists to push between field lines on neighboring flux surfaces on the outboard side while remaining unperturbed from its original location far along the field line.

MAST is well equipped with diagnostics for the study of ELMs [10], which have a typical duration $\sim$200 μs. During this time, heat and particles are ejected from the confined plasma into the scrape-off layer and then travel along the field lines to the target plates. The cool deuterium atoms at the plasma periphery and those released from the target by recycling are excited through collisions with the expelled plasma. The consequent burst of Balmer α-series (D_α) light together with the detection of heat and particles arriving at the divertor target plates are characteristic signatures of the ELM event.

A previous study [11] has shown no significant difference in the time of peak D_α emission at the upper and lower X points or outboard midplane suggesting that the particles responsible for producing the D_α emission arrive simultaneously at the midplane and upper and lower X points. This suggests that the ELM process is not only up-down symmetric but also that it is extended in the poloidal direction.

The first evidence for the toroidal localization and radial extent of the ELM outside of the plasma comes from a reciprocating Langmuir probe, which measures the ion flux at the outboard midplane in the scrape-off layer [10]. Figure 1(a) shows a plot of the divertor D_α and the ion saturation current density (J_{SAT}) observed at the reciprocating probe where the probe was at a distance $\Delta_r \sim 3$ cm from the plasma edge. The rise in J_{SAT} is delayed with respect to the rise in target D_α emission. This delay increases with Δ_r and can be used to calculate a mean radial expansion velocity away from the separatrix, $v_r \sim 750\ \mathrm{ms}^{-1}$. Figure 1(b) shows a plot of the power density arriving at the probe as a function of distance between the probe and the plasma edge. The observed power density can be considerable for $\Delta_r <$ $\sim$10–15 cm and can still be $> 10\%$ of the peak value observed at the divertor target probes up to 20 cm from the plasma edge. As can be seen from Fig. 1(a), during a single ELM, two or three distinct periodic peaks in the ion flux are observed decreasing in amplitude. Each one lasts for $\sim$5–10 μs and they are separated by

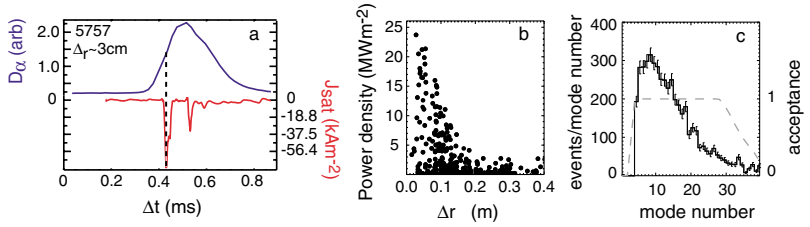

FIG. 1 (color online). (a) The D_α signal and the J_{SAT} observed at the reciprocating probe. (b) The power density of ELM efflux observed at the midplane reciprocating probe as a function of distance from the plasma edge. (c) The distribution of derived mode number (the dashed curve shows the results of a simulation of the spectral acceptance).

$\Delta t \sim 45$–50 μs. The toroidal rotation velocity of the plasma edge is typically $V_{ped} \sim 15$ km s^{-1}. These features are consistent with the nonlinear ballooning mode theory [8,9], which predicts that the ELM is composed of several narrow plasma filaments that project out into the scrape-off layer at the outboard midplane. Such a filamentary structure would also explain the apparently poloidally extended nature of the ELM needed to explain the D_α observations and the scatter in power density at a given radius [Fig. 1(b)] due to the toroidal location of the probe with respect to where the filament originates. Interpreting the J_{SAT} peaks as filaments rotating with the plasma past the probe, these results shown in Fig. 1(a) give a filament width of ~7.5–15 cm and a toroidal separation between filaments of ~75 cm. The toroidal circumference around the outside of the plasma is typically $L_{outer} \sim 9$ m implying that the structure has a toroidal mode number $= L_{outer}/(V_{ped}\Delta t)$ in the region ~12. This is consistent with the most unstable modes typically predicted by the linear theory of ideal magnetohydrodynamics [12]. The toroidal mode number has been derived for a range of ELMs where the probe was less than 5 cm from the plasma edge and the time difference, Δt, was in the range $20\ \mu s < \Delta t < 200\ \mu s$. Figure 1(c) shows the distribution of derived toroidal mode numbers for a range of ELMs. The peak in the distribution is 9 and the mean is 15. This mode structure is similar to that inferred from infrared camera measurements of the toroidal and radial structure observed in power deposition profiles at the target plates in ASDEX Upgrade [13]. To determine the effect of the time range restriction ($20\ \mu s < \Delta t < 200\ \mu s$) on the spectral response, a simulation has been performed and the resulting acceptance is shown superimposed on Fig. 1(c) as a dashed line. The cut of $\Delta t < 200\ \mu$s results in effectively zero acceptance for mode numbers <4. The cut $\Delta t > 20\ \mu$s produces a drop in acceptance for mode numbers above 30; however, the rest of the distribution is unaffected.

Further evidence for the filamentary nature of the ELM and its temporal evolution comes from the high resolution ruby laser Thomson scattering system on MAST (the spatial and temporal resolution are 3 mm and 30 ns, respectively [14]). Once per shot, this system produces the electron density and temperature profiles across the midplane of the plasma. Figure 2(a) shows a typical outboard density profile obtained just before an ELM ($t_{ELM} - 740\ \mu$s); the core density profile is very flat with a steep edge density. t_{ELM} is defined as the start of the ELM and, in this instance, is determined from the time at which the midplane D_α signal increases by 10% of the value at the ELM peak. A study of the Thomson scattering density profiles obtained during the rise time of the midplane D_α signal (typically 200 μs) shows that the ELM has very little impact on the inboard side, but reduces the density gradient on the outboard side. These observations are consistent with the ballooning mode theory of ELMs [4]. Of the 40 discharges analyzed thus far, six show the formation of a broad outboard tail in both the density [Fig. 2(b) obtained at $t_{ELM} + 140\ \mu$s] and the temperature distribution and four exhibit a distinct structure in the density distribution in the scrape-off layer on the outboard side [at a radius of ~1.4 m in Fig. 2(c) obtained at $t_{ELM} + 180\ \mu$s]. The reason why most profiles see no tail will be explained below. This structure is also observed by a linear camera, detecting D_α light at different radial locations [11].

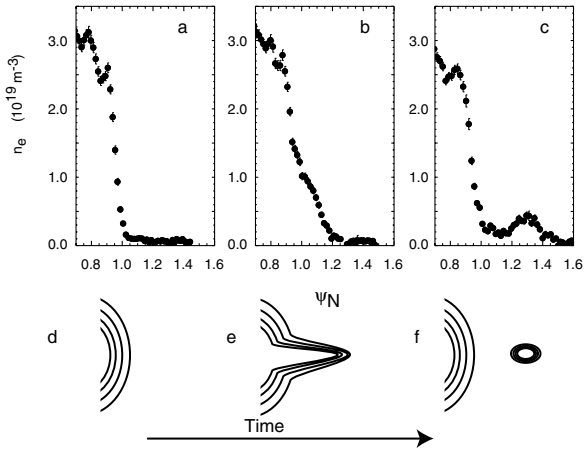

FIG. 2. Thomson scattering profiles of the outboard edge density in normalized flux coordinates at different times with respect to the start of a similar ELM. (a) Before ($t_{ELM} -$ 770 ms), (b) in the middle of the ELM rise ($t_{ELM} + 140$ ms), and (c) near the end of the ELM rise time ($t_{ELM} + 180$ ms). A schematic of the proposed magnetic geometry in the poloidal cross section at the outboard plasma edge for the same time periods is shown in (d), (e), and (f), respectively.

The Thomson scattering data can be understood if the structures observed are radially perturbed plasma filaments. Since the Thomson scattering system makes measurements at a specific toroidal location and specific time, whether or not the filament is detected depends on its toroidal location at the time that the data is collected (the filament would rotate with the plasma). The reciprocating probe data implies a typical toroidal mode number of $n = 12$ and a filament width of 15 cm. Taking an outer radius of the plasma of 900 cm means that the ELM toroidal coverage is $\sim 180/900 \sim 20\%$ of the outboard surface at the midplane. This explains why the structure in the scrape-off layer is observed only by the Thomson scattering system 10 times in 40 discharges.

The following is a possible interpretation of the experimental observations. During the inter-ELM period, steep gradients in both density and temperature develop just inside the separatrix in the pedestal region, reaching a peak shortly before the ELM [Fig. 2(a) shows a typical density profile]. At this time, the axisymmetric magnetic geometry is unperturbed [Fig. 2(d)]. At the onset of the ELM, narrow plasma filaments develop, locally perturbing the outboard separatrix and flux surfaces in the scrape-off layer [Fig. 2(e)]. Although these are extended along a field line, the perturbations appear to be poloidally localized at any particular toroidal angle. Thomson scattering measurements during this time, and for which the perturbation is in the field of view, show a flattening of the edge gradients. This is typically seen most clearly in the density profile, which forms a broad outboard tail [Fig. 2(b)]. Disturbance to the outboard flux surfaces leads to enhanced cross-field transport of heat and particles into the scrape-off layer. Finally, by magnetic reconnection, the filament detaches from the core at the midplane [Fig. 2(f)], though possibly still remaining attached closer to the X-point region. Thomson scattering measurements with the correct spatial and temporal phasing now show a discrete, outboard density peak [Fig. 2(c)]. Since the filament, at least in the early stages, is linked to the core, the amount of energy in the plasma volume occupied by the filament is less than the amount of energy lost due to the ELM. During this time, the filament acts as a conduit for losses from the pedestal region by distorting the outboard flux surfaces. The amount of plasma energy in the volume occupied by the filament during the phases indicated in Figs. 2(b), 2(e), 2(c), and 2(f) can be calculated using $W_{\text{filament}} = \frac{3}{2} n_e (T_e + T_i) V_{\text{filament}}$ and assuming $T_i = T_e$. V_{filament} is the volume of the filament calculated using the length of the filament assuming it follows the q_{95} surface and extends from X point to X point, having a toroidal extent of 15 cm (consistent with the data from the reciprocating probe) and a radial extent given by the density profile. The estimated energy contained in each filament is 4 J [Fig. 2(b)] and 1.2 J [Fig. 2(c)] given by the measured density profile perturbation. Even assuming that there could be 10–15 filaments, the total energy content (<60 J) is only a small fraction of the energy loss due to this ELM of ~ 500 J. Hence, this shows that the filament is not a blob of plasma that is breaking away from the core but is a finger that connects back to the core, providing a path for the heat to escape from the core to the scrape-off layer.

The data presented in Fig. 2 come from different ELMs in different discharges. Further evidence for the time evolution of the ELM filament comes from data from the multitime point Nd-doped yttrium aluminum garnet (Nd:YAG) Thomson scattering system on MAST that can be arranged to give four electron density and temperature radial profiles during a single ELM. An example is shown in Fig. 3. Although the spatial resolution is poorer in this case (~ 3 cm), the general features described in Fig. 2 can be observed, namely, a steep gradient before the ELM (solid circle), followed by a broad outboard tail (open circle). This is then followed by a decrease in the density pedestal, withdrawal of the outboard tail, and possible production of a localized density structure at 1.435 m (closed squares). Finally (open squares), all perturbations outside the last closed flux surface (LCFS) disappear and just the decrease in pedestal density and gradient remain. From the 36 ELMs studied that have at least one profile obtained during the rise time of the ELM, nine show the clear production of an outboard density tail which is again consistent with the toroidal coverage of the ELM described above.

All the data we have described thus far can provide only a one-dimensional view around the plasma midplane. To confirm the filamentary structure requires a two-dimensional measurement. This final evidence comes from a unique capability on MAST to view a large fraction of the plasma surface and, hence, obtain a photograph of an ELM using a high-speed camera with a short (20 μs) exposure time. Provided the plasma rotation is sufficiently slow so that the features are not blurred, clear filaments are observed [Fig. 4(a)].

These filaments are consistent with the structure expected from the nonlinear ballooning mode theory illustrated in Fig. 4(b). This theory predicts that the ballooning mode grows explosively and evolves into a filament of plasma, localized about a particular magnetic

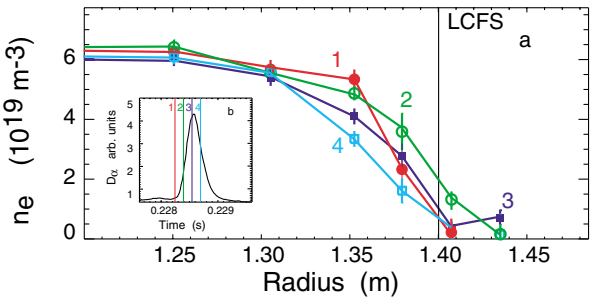

FIG. 3 (color online). (a) The time evolution of the edge density profile for a single ELM. (b) (inset) The target D_α signal indicating the time of the density profile relative to the ELM.

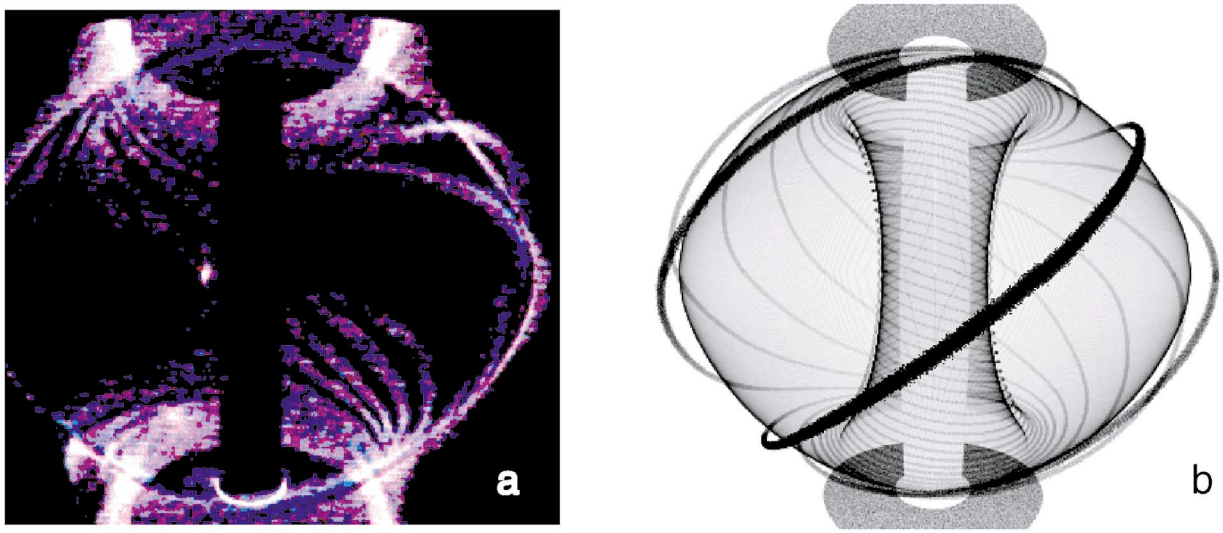

FIG. 4 (color). (a) High-speed video image of the MAST plasma obtained at the start of an ELM. (b) The predicted structure of an ELM in the MAST tokamak plasma geometry, based on the nonlinear ballooning mode theory.

field line, which narrows and twists as it is ejected from the plasma on a time scale $\sim(\tau_A^2\tau_E)^{1/3}$ (τ_A is the Alfvén time and τ_E is the energy confinement time of the plasma [15]). Taking a typical energy confinement time on MAST of 50 ms and an Alfvén time of 5 μs gives $\sim$110 μs for the growth time. During this time, plasma from the hot core will flow rapidly along field lines in the filament, providing a path for heat and particles to escape from the confined core into the scrape-off layer region. τ_{MHD} is the time over which particles are leaving the core plasma due to the ELM and for MAST $\tau_{\mathrm{MHD}} = 87 \pm 25$ μs [10], which is in good agreement with the filament growth time predicted above. In MAST τ_{MHD} is less than or equal to the parallel transport time of the ELM ($\tau_{\|} \sim$ 120–150 μs) and, hence, the ELM event is almost finished before the ions ejected from the ELM have reached the target. According to Ref. [16], this scenario should lead to the ELM energy losses in MAST being convective in nature as is observed [17].

Taken together, the observations presented in this Letter provide strong evidence for the ELM being a filamentlike structure, which is extended along a field line in such a way that at any toroidal angle it appears to be poloidally localized and at any poloidal position it appears to be toroidally localized. Filamentary structures, generated on a 100 μs time scale, erupt from the outboard side and connect back into the plasma. This filament is observed on several diagnostics to extend beyond the separatrix, and ELM effluxes are observed radially up to 20 cm from the plasma edge. For the first time, a high-speed picture has been obtained of an ELM showing this filamentlike structure. Such a structure would be expected from the theory of the nonlinear evolution of ballooning modes, adding support to the idea that peeling-ballooning modes are responsible for triggering ELM events. Furthermore, the visual similarity between the ELM structure [see the top right-hand part of Fig. 4(a)] and some forms of solar eruptions is tantalizing. It raises the question of whether or not the ballooning mode could indeed play a role in both phenomena, as proposed by theory [9].

We thank Jack Connor, William Morris, and Martin O'Brien for helpful comments on the manuscript. This work was funded jointly by the United Kingdom Engineering and Physical Sciences Research Council and by EURATOM.

[1] J.W. Connor, Plasma Phys. Controlled Fusion **40**, 531 (1998).
[2] W. Suttrop, Plasma Phys. Controlled Fusion **42**, A1 (2000).
[3] J.W. Connor, R. J. Hastie, and J. B. Taylor, Proc. R. Soc. London, Ser. A **365**, 1 (1979).
[4] J.W. Connor, R. J. Hastie, H. R. Wilson, and R. L. Miller, Phys. Plasmas **5**, 2687 (1998).
[5] A.W. Hood, Sol. Phys. **103**, 329 (1986).
[6] P. Gohil *et al.*, Phys. Rev. Lett. **61**, 1603 (1988).
[7] B. Lloyd *et al.*, Nucl. Fusion **43**, 1665 (2003).
[8] O. A. Hurricane, B. H. Fong, and S. C. Cowley, Phys. Plasmas **4**, 3565 (1997).
[9] H. R. Wilson and S. C. Cowley, Phys. Rev. Lett. (to be published).
[10] A. Kirk *et al.*, Plasma Phys. Controlled Fusion **46**, 551 (2003).
[11] A. Kirk *et al.*, Europhysics Conference Abstracts 27A (2003), Session P-3.201.
[12] P. B. Snyder *et al.*, Phys. Plasmas **9**, 2037 (2002).
[13] T. Eich *et al.*, Phys. Rev. Lett. **91**, 195003 (2003).
[14] M. J. Walsh *et al.*, Rev. Sci. Instrum. **74**, 1663 (2003).
[15] S. C. Cowley and M. Artun, Phys. Rep. **283**, 185 (1997).
[16] A.W. Leonard *et al.*, J. Nucl. Mater. **313–316**, 768 (2003).
[17] A. Kirk *et al.*, Plasma Phys. Controlled Fusion **46**, A187 (2004).